Structure of complex systems using electronic excitation transport: Theory, Monte Carlo simulations, and experiments on micelle solutions

Karin U. Finger, Andrew H. Marcus, and M. D. Fayer
Department of Chemistry, Stanford University, Stanford, California 94305

(Received 2 August 1993; accepted 14 September 1993)

Monte Carlo (MC) simulations and an analytical theory are presented to describe electronic excitation transport (EET) among static chromophores constrained to lie on the surfaces of spherical micelles. Both donor–trap (DT) and donor–donor (DD) EET are examined for two types of systems: probe molecules on the surfaces of isolated (low concentration) micelles, and probes on the surfaces of interacting (concentrated) micelles. The EET dynamics are described by the function, $\langle G^s(t)\rangle$, the probability of finding the excitation on the originally excited chromophore. For the isolated micelle calculations, the excitation dynamics depend on the distribution of probes on a single hard sphere surface. For the interacting micelle calculations, the hard sphere structure is accounted for by using the radial pair distribution function, $g(r)$. Both single micelle and many micelle DT calculations do not involve approximations. Consequently, the DT expressions agree exactly with the MC calculations. For the DD calculations, a first order cumulant approximation is used to obtain analytically tractable solutions to $\langle G^s(t)\rangle$. Padé approximants of the cumulant solution, accurate over a broad range of chromophore number and Förster interaction strengths, are used to describe DD EET on isolated micelles. For DD EET in many micelle systems, the first order cumulant approach is shown to be a suitable method for intermicelle structural studies. Both the cumulant and MC calculations are simultaneously compared to time resolved flourescence depolarization measurements performed on octadecylrhodamine B(ODRB)/triton X-100/water systems made in previous investigations.

I. INTRODUCTION

The theory and application of electronic excitation transport (EET) to nonrandom chromophore distributions has led to new routes for the structure elucidation of complex systems.[1–13] Studies of donor–donor EET among chromophores bound to polymer coils and to micelle assemblies have been used to quantitatively measure the rms radius of gyration of the polymer,[14] and the average micelle radius.[15,16] Both of these measurements are intramolecular or intramicellar quantities. They depend on the clustered distribution of chromophores on a single polymer molecule or micelle.

Recently, an analytical method has been developed to describe EET among interacting clusters of chromophores.[2] The technique has been applied to experimental studies of concentrated micelle suspensions with chromophores constrained to lie at the micelle surfaces,[16] and to pendant chromophores covalently bound to the backbones of interpenetrating polymer chains.[17] The surface micelle system was constructed with octadecylrhodamine B(ODRB) in triton X-100 micelles; the tagged polymer system by a copolymer consisting of methyl methacrylate and 2-vinyl naphthalene subunits. In both situations, EET occurs within a chromophore cluster (e.g., a micelle or polymer coil) and between clusters.

The method makes use of a truncated cumulant approximation which is based on the assumption that the cumulative effect of all transfer processes is well described by a superposition of pair wise interactions.[11,18–20] In this way, the multiple step processes which occur in clustered systems may be partitioned into fast events internal to a cluster and the slower transfer steps between interacting clusters. This renormalizes a many-body problem into a tractable two-body problem that can be formulated analytically. Since the interaction between clusters is treated in analogy to the interaction between two "effective chromophores," the technique is called the effective chromophore (EC) method.

For the polymer system mentioned above,[17] the analysis of the experimental data supplied information about the intermolecular segmental distribution function (sometimes referred to in the literature as the correlation hole). In that study, the theoretical predictions for the experimental measurements were *quantitatively* accurate. For the case of the micelle system, however, only qualitative agreement between theory and data was observed. The intermicelle EET experimental observable, which depends on the micelle solution structure, was found to have a somewhat different time dependence than that predicted by the theory.

As discussed in Ref. 16, there are a number of possible causes for this disagreement. For the theory to reproduce the micelle data accurately, at least two conditions must be met.

(i) The chromophore configurations are well described as noninteracting probes on the surfaces of spherical micelles which are located in solution as in a hard sphere liquid.[21]

(ii) Given a suitable distribution of configurations, the first order cumulant and the EC method accurately predict the experimental observables.

 0021-9606/94/100(1)/271/16/$6.00

Statement (i) reflects the model dependency of the analysis. It implies that other chromophore distributions may describe the experimental situation better. However, a meaningful structural interpretation of the data is not possible until the validity of statement (ii) has been tested.

In Ref. 16, information concerning the probe morphology in *isolated* micelle systems was extracted from the experimental data. This was possible because the results of the cumulant theory for intramicelle EET was checked against Monte Carlo (MC) calculations. Comparison between the validated theory and data at higher chromophore concentrations suggested the repulsive nature of the intermolecular potential between probe molecules. Interactions between probe molecules were accounted for by skewing the occupation distribution towards fewer chromophores per micelle. In a similar fashion, it is possible to examine the accuracy of the EC method for intermicelle EET by comparison with MC simulation.

The generation of suitable probe configurations consistent with the hard sphere model is readily accomplished using MC simulation. The problem is approached in two steps. First, a viable configuration of spheres is achieved using standard MC methods.[22] Second, probe molecules are chosen so that they lie randomly on the spherical surfaces. The excitation transport dynamics are then uniquely determined by the set $\{\mathbf{r}\}$, containing the probe coordinates.[23] These dynamics are completely described by the self part of the Green's function solution to the transport master equation, $G^s(t)$.[24] $G^s(t)$ is the diagonal portion of the Green's function. It represents the probability that the originally excited chromophore is still excited at some later time. $G^s(t)$ includes transfer events in which the excitation leaves the initial site and later returns. Direct numerical computation of the transport master equation leads to an exact solution for $G^s(t)$ for a given configuration. This process is repeated many times, with each subsequent iteration representing an additional contribution to the configurational average, $\langle G^s(t)\rangle$.

The usefulness of $\langle G^s(t)\rangle$ lies in its relationship to the observables obtained from fluorescence depolarization experiments. A polarized excitation of an ensemble of randomly oriented chromophores results in a photoselective excited state. Only chromophores with the appropriate transition dipole vectors can be initially excited. Transfer of the excitation to surrounding molecules, which are randomly oriented, and subsequent emission by the excited molecule leads to depolarization of the observed fluorescence. This results in fluorescence anisotropies dominated by $\langle G^s(t)\rangle$ provided other depolarization processes (such as chromophore rotation) occur on a slower time scale. In the present work, we make the approximation that chromophore motion occurs slowly enough to neglect its effect on the EET observable. This is an acceptable simplification of the model since we are primarily interested in testing the accuracy of the first order cumulant approach. Recent evidence, however, suggests that chromophore motion directed along the micelle surface is significant.[25] Lateral diffusion constants have been measured that correspond to mean squared displacements comparable to the micelle dimension. The effect of chromophore motion on the EET observable is a current topic of investigation.[26]

In this paper, we present Monte Carlo simulations of EET among chromophores constrained to lie at the surfaces of dilute and concentrated solutions of spherical micelles. For the isolated micelle case, the MC results are compared to the first order cumulant approximation of $\langle G^s(t)\rangle$ that has been improved with Padé approximants.[16] For the highly concentrated micelle systems, the simulations are compared to the analytical results predicted by the EC method. Analytical and MC results are compared together with experimental data previously reported in Ref. 16.

This paper is organized in the following manner: In Sec. II, we briefly describe the two-particle cumulant approximation and the EC method as applied to donor–donor EET. For the purpose of comparison, we present the analogous donor–trap calculations. Section III contains a discussion of the MC calculations applied to chromophore–micelle systems (specifically, the ODRB/triton X-100/water systems). In Sec. IV, we discuss the results and make comparisons to experimental data.

II. ANALYTICAL THEORY OF EET IN HARD SPHERE MICELLES

There are two important categories of experimentally accessible EET systems: donor–donor and donor–trap. Donor–donor systems (DD) involve energy transport among chemically identical chromophores. This means all the chromophores have similar energies such that the excitation can "hop" from site to site. Thus the trajectory of an initial excitation may follow a complicated pathway among sites before a radiative process (fluorescence) can occur. Donor–trap systems (DT) characteristically describe direct energy transport between two chemically distinct species. The "donor" chromophore is selectively excited and transfer of the excitation to a "trap" is irreversible. In a DT system, there can be no significant back transfer to the donor.

Both DD and DT systems are characterized by the behavior of $\langle G^s(t)\rangle$. For the case of DD transport, the derivation of an analytical expression for $\langle G^s(t)\rangle$ requires approximations due to the infinite number of possible excitation pathways. The accuracy of the expression depends on the validity of the approximations. In a DT system, however, there are a finite number of possible pathways, and consequently an analytical expression for $\langle G^s(t)\rangle$ represents an *exact* description of the excitation dynamics. Since the MC calculations presented below attempt to describe DD dynamics exactly, analogous DT calculations serve as a useful self-consistency check of the numerical procedures.

General analytical treatments of DD and DT EET have been presented elsewhere.[2,11,12,16,27] Therefore, only the essential expressions specifically derived for hard sphere systems are given here. The reader is referred to the original sources for more details. Two types of configurational situations are considered: isolated spherical micelles and concentrated solutions of spherical micelles.

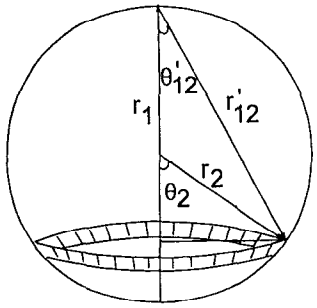

FIG. 1. A micelle is modeled as a sphere centered at the origin with radius R_m. The vectors $\mathbf{r}_1$ and $\mathbf{r}_2$ specify the locations of two probe molecules on the micelle surface. The meanings of the variables θ_2, θ'_{12}, and r'_{12} are shown.

A. Single micelle systems

1. One donor and N−1 traps randomly distributed on a spherical surface

The general expression for a system of one donor interacting with $N-1$ traps is[27]

$$\langle G^s(t)\rangle = \int_{\mathbf{r}_1} P(\mathbf{r}_1)d\mathbf{r}_1 \int_{\mathbf{r}_2} P(\mathbf{r}_2)\exp[-\omega(\mathbf{r}_{12})t]d\mathbf{r}_2 \times \int_{\mathbf{r}_3} P(\mathbf{r}_3)\exp[-\omega(\mathbf{r}_{13})t]d\mathbf{r}_3 \cdots \int_{\mathbf{r}_N} P(\mathbf{r}_N) \times \exp[-\omega(\mathbf{r}_{1N})t]d\mathbf{r}_N. \quad (2.1)$$

In Eq. (2.1), the donor is labeled by position 1 and the traps by positions 2 through N. The rate constant, $\omega(\mathbf{r}_{1i})$, is given by

$$\omega(\mathbf{r}_{1i}) = \frac{1}{\tau_F}\left(\frac{\gamma^{1/2}R_0^{\mathrm{DT}}}{r_{1i}}\right)^6, \quad (2.2)$$

where R_0^{DT} is the Förster critical transfer distance for direct trapping, $\gamma^{1/2}(=0.9202)$ is the dynamic orientational factor, and r_{1i} is the absolute distance between the donor and the ith trap, and τ_F is the radiative fluorescence lifetime. For an isolated sphere, all the traps are described by the same spatial distribution, so that Eq. (2.1) becomes

$$\langle G^s(t)\rangle = \int_{\mathbf{r}_1} P_d(\mathbf{r}_1)d\mathbf{r}_1\left(\int_{\mathbf{r}_2} P_t(\mathbf{r}_2) \times \exp[-\omega(\mathbf{r}_{12})t]d\mathbf{r}_2\right)^{N-1}, \quad (2.3)$$

where $P_d(\mathbf{r}_1)$ is the spatial distribution of the donor molecule and $P_t(\mathbf{r}_2)$ is that of the traps. Consider the sphere to have a radius, R_m, with its center at the origin (see Fig. 1). Since all positions on the surface are translationally invariant, the integration over donor positions in Eq. (2.3) can be eliminated

$$\langle G^s(t)\rangle = \left(\int_{\mathbf{r}_2} P(\mathbf{r}_2)\exp[-\omega(\mathbf{r}_{12})t]d\mathbf{r}_2\right)^{N-1}. \quad (2.4)$$

It is shown in Appendix A that the integral in Eq. (2.4) has the analytical solution

$$\langle G^s(t)\rangle = [\mu^{1/3}\gamma(2/3,\mu) - \mu^{1/3}\Gamma(2/3) + \exp(-\mu)]^{N-1}, \quad \text{DT; single sphere,} \quad (2.5)$$

where $\mu = 2Q^6 t/\tau_F$, $Q = R_0^{\mathrm{DT}}/2R_m$, and $\Gamma(2/3) = 1.254\,117\,94$. $\Gamma(a)$ and $\gamma(a,x)$ are the complete and incomplete Euler gamma functions, respectively, defined by

$$\Gamma(a) = \int_0^\infty e^{-t}t^{a-1}\,dt, \quad \gamma(a,x) = \int_0^x e^{-t}t^{a-1}\,dt.$$

Equation (2.5) is an exact representation of this single sphere DT problem for any number of traps.

2. N donors randomly distributed on a spherical surface

The cumulant approximation for DD transport on the surface of a single sphere has been reported previously.[2,16] This is based on the assumption that all transfer events between chromophores are due to pairwise interactions. Two-particle approximations of this type are in excellent agreement with more accurate representations of the Green's function for infinite isotropic systems as well as some restricted finite volume systems.[12,14,18–20] With this approach, an excitation that leaves the originally excited chromophore can only repopulate the original site by returning directly after the first step (a two-particle interaction). Unlike the second-order density expansion of Ediger *et al.*,[15] there is no possibility of a third chromophore acting as a bridge site (a three-particle interaction). Thus the cumulant expression for DD transport on a single spherical surface reduces to the exponential of a surface integral similar to Eq. (2.4)

$$\langle G^s(t)\rangle = \exp\left(\int_{\mathbf{r}_2} P(\mathbf{r}_2)\exp[-\omega(\mathbf{r}_{12})t - 1]d\mathbf{r}_2\right), \quad (2.6)$$

where

$$\omega(\mathbf{r}_{12}) = \frac{1}{\tau_F}\left(\frac{\gamma^{1/2}R_0^{\mathrm{DD}}}{r_{12}}\right)^6,$$

R_0^{DD} is the DD critical transfer distance, and $\gamma^{1/2}$ is defined as in Eq. (2.2). The analytical solution of Eq. (2.6) is given by

$$\langle G^s(t)\rangle = \exp\left(\frac{(N-1)}{2}[\mu^{1/3}\gamma(2/3,\mu) - \mu^{1/3}\Gamma(2/3) + \exp(-\mu) - 1]\right) \quad \text{DD; single sphere.} \quad (2.7)$$

μ, γ, and Γ are defined as in Eq. (2.5). Equation (2.7) is accurate for short time and weak interactions (e.g., small $Q = R_0^{\mathrm{DD}}/2R_m$). However, at long time or for strong interactions Eq. (2.7) becomes increasingly inaccurate because it approaches an unrealistic asymptotic limit,

$$\text{as } t \to \infty, \quad \text{Eq. (3.6)} \to \exp\left(\frac{1-N}{2}\right) \quad (2.8)$$

instead of the correct value, $1/N$. For this reason, Padé approximants[28] were constructed from Eq. (2.7). These functions preserve the short time (or weak interaction) behavior of the cumulant, but replace the asymptotic (or strong interaction) behavior with the correct value. Padé approximants accurate for values of N over the range [0,15] and for Q over the range [0,1.3] are presented in Appendix B.

B. Many micelle systems

1. One donor and N−1 traps randomly distributed on the surfaces of many spheres

We assume a system of spheres that contain a donor chromophore and $N-1$ traps. The chromophores are noninteracting so that the number of probes on a given sphere follows from a Poisson function.[16] The distribution of traps seen by the donor fall into two categories: those that occupy the same sphere as the donor and those that occupy neighboring spheres. In this case, Eq. (2.1) can be rewritten,

$$\langle G^s(t)\rangle = \int_{r_1} P_d(\mathbf{r}_1)d\mathbf{r}_1\left(\int_{r_2} P_{\text{t-on}}(\mathbf{r}_2) \times \exp[-\omega(\mathbf{r}_{12})t]d\mathbf{r}_2\right)^m\left(\int_{r_3} P_{\text{t-off}}(\mathbf{r}_3) \times \exp[-\omega(\mathbf{r}_{13})t]d\mathbf{r}_3\right)^n. \tag{2.9}$$

The distributions $P_{\text{t-on}}(\mathbf{r})$ and $P_{\text{t-off}}(\mathbf{r})$ correspond to the trap positions on the sphere containing the donor and those on neighboring spheres, respectively. In Eq. (2.9), m is the number of traps on the donor sphere and n is the number on all other spheres, such that $m+n=N-1$. Equation (2.9) suggests the factorization of the Green's function into internal and external parts

$$\langle G^s(t)\rangle = \langle G^s_{\text{on}}(t)\rangle\langle G^{(s)}_{\text{off}}(t)\rangle. \tag{2.10}$$

Here $\langle G^s_{\text{on}}(t)\rangle$ is the survival probability of the donor excitation due to transfer to traps on the same sphere. [This is given by a Poisson average of Eq. (2.5).] Transfer of the excitation to traps off the original sphere is given by

$$\langle G^s_{\text{off}}(t)\rangle = \int_{r_1} P_{\text{d-on}}(\mathbf{r}_1)d\mathbf{r}_1\left(\int_{r_2} P_{\text{t-off}}(\mathbf{r}_2) \times \exp[-\omega(\mathbf{r}_{12})t]d\mathbf{r}_2\right)^n, \tag{2.11}$$

where the subscript 3 has been replaced with a 2 for simplicity. In order to evaluate Eq. (2.11), the space spanned by the vector $\mathbf{r}_2$ must be expressed in terms of the one spanned by $\mathbf{r}_1$. This is accomplished by writing $P_{\text{t-off}}(\mathbf{r})$ as the product of two joint distributions. One describes the locations of trap molecules on another sphere separated from the original by a distance, R_s. The other describes the distribution of sphere separations.

$$P_{\text{t-off}}(\mathbf{r}_2) = P_{\text{t-off}}(\mathbf{r}_2;R_s)\cdot P_{\text{sphere}}(R_s), \tag{2.12}$$

where $P_{\text{t-off}}(\mathbf{r}_2;R_s)$ is the pairwise distribution of traps on an "acceptor" sphere relative to the distribution of a single donor on a "donor" sphere, and $P_{\text{sphere}}(R_s)$ is related to the hard sphere radial distribution function, $g(R_s)$. Equation (2.11) can then be rewritten,

$$\langle G^s_{\text{off}}(t,R_s,n_p)\rangle = \int_{r_1} P_{\text{d-on}}(\mathbf{r}_1)d\mathbf{r}_1\left(\int_{r_2} P_{\text{t-off}}(\mathbf{r}_2;R_s) \times \exp[-\omega(\mathbf{r}_{12})t]d\mathbf{r}_2\right)^{n_p}. \tag{2.13a}$$

Equation (2.13a) describes the decay of exitation probability due to intersphere EET for a pair of spheres separated by the distance, R_s, and with n_p trap molecules on the acceptor sphere. Since micelles are dynamic assemblies of molecules, which constantly gain or lose constituents, a distribution function, $P(n_p)$, is used to describe the probability of finding n_p chromophores on a given micelle. In general, this distribution depends on the effect of chemical forces between the chromophores.[16] For the simple case of noninteracting chromophores, $P(n_p)$ is given by the Poisson distribution. The Poisson average of Eq. (2.13a) is

$$\langle G^s_{\text{off}}(t,R_s,\nu)\rangle = \sum_{n_p=0}^{\infty}\frac{n_p}{\nu}\left(\frac{e^{-\nu}\nu^{n_p}}{n_p!}\right)\langle G^s_{\text{off}}(t,R_s,n_p)\rangle, \tag{2.13b}$$

where ν is the mean occupation number of chromophores per micelle. Equations (2.13a) and (2.13b) contain ensemble averages over the internal chromophore structure of two micelles. The intermicelle structure is described by an ensemble average over space, weighted by the radial pair distribution function

$$\langle G^s_{\text{off}}(t,\nu)\rangle = \left(\frac{4\pi}{V}\int\langle G^s_{\text{off}}(t,R_s,\nu)\rangle g(R_s)R_s^2\,dR_s\right)^{n_s-1}. \tag{2.13c}$$

In Eq. (2.13c), n_s is the total number of hard spheres in the integration volume V. The specific integrals in Eq. (2.13a) must be evaluated by numerical methods. They have been examined previously[2] and shown to simplify to

$$\langle G^s_{\text{off}}(t,R_s,n_p)\rangle = \frac{1}{2}\int_{\theta_1}\sin\theta_1\,d\theta_1 \times\left(\frac{1}{2}\int_{\theta_2}\exp[-\omega(\mathbf{r}'_{12}(\theta'_{12},\theta_2,R_s))t] \times\sin\theta_2\,d\theta_2\right)^{n_p}, \tag{2.14a}$$

where

$$\theta_2 = \theta'_{12}+\arcsin\left(\frac{r^0_{12}\sin\theta'_{12}}{R_m}\right)-\arcsin\left(\frac{R_m\sin\theta_1}{r^0_{12}}\right), \tag{2.14b}$$

$$d\theta_2 = \left(1+\frac{r^0_{12}\cos\theta'_{12}}{R_m[1-(r^0_{12}\sin\theta'_{12}/R_m)]}\right), \tag{2.14c}$$

$$r'_{12}(\theta'_{12},\theta_1)=\cos\theta'_{12}\, r^0_{12}(\theta'_{12},\theta_1) \pm[\cos^2\theta'_{12}(R_m^2+2R_mR_s\cos\theta_1) -(R_s^2+2R_mR_s\cos\theta_1)]^{1/2}, \quad (2.14d)$$

and

$$r^0_{12}(\theta'_{12},\theta_1)=[R_m^2+R_s^2-2R_mR_s\cos\theta_1]^{1/2}. \quad (2.14e)$$

In practice, Eqs. (2.14) are numerically evaluated for several values of n_p and R_s. The Poisson average, Eq. (2.13b) is substituted into Eq. (2.13c) and finally into Eq. (2.10) to obtain $\langle G^s(t)\rangle$. This is an exact solution to the DT problem for a system of interacting hard spheres.

2. N donors randomly distributed on the surfaces of many spheres

The cumulant approximation for DD EET among chromophores distributed on interacting spherical surfaces was introduced by Marcus *et al.*[2,16] For DD transport, the expression given by Eq. (2.10) is an approximation which strictly follows from the cumulant theory. $\langle G^s_{\rm on}(t)\rangle$ is given by the Poisson average of Eq. (2.7). $\langle G^s_{\rm off}(t)\rangle$ is calculated as a configurational integral over pairwise interactions in direct analogy to the DT formulation presented above. The most notable differences between the DT and DD formulations are the following: Eqs. (2.14a) is replaced with

$$\langle G^s_{\rm off}(t,R_s,n_p)\rangle = \frac{1}{2}\int_{\theta_1}\sin\theta_1\, d\theta_1 \exp\Bigg(\frac{(N-1)}{4} \times\int_{\theta_2}\exp\{-2\omega[r'_{12}(\theta'_{12},\theta_2,R_s)]t -1\}\sin\theta_2\, d\theta_2\Bigg), \quad (2.15)$$

and Eq. (2.13c) is replaced with

$$\langle G^s_{\rm off}(t)\rangle = \exp\Bigg(-\frac{4\pi n_s}{V}\int[1-\langle G^s_{\rm off}(t,R_s)\rangle]g(R_s)R_s^2\, dR_s\Bigg). \quad (2.16)$$

Definitions of $r'_{12}(\theta'_{12},\theta_2,R_s)$, $\sin\theta_2$, and $d\theta_2$ are defined as in Eqs. (2.14). $\langle G^s(t)\rangle$ is then calculated exactly as described for the DT problem.

In the many sphere problem, the exclusion of three-particle or n-particle interactions have additional consequences to those discussed for the single sphere DD system above. Pathways that involve a bridge chromophore are not included in this calculation of $\langle G^s(t)\rangle$. Bridge chromophores may be located on the acceptor sphere, on the original donor sphere, or on a third "bridge sphere." The accuracy of this approximation can now be checked by comparison to MC calculations which include all possible pathways.

C. Continuum model for the radial distribution of a hard sphere micelle system

For the purposes of this work, the relative spatial locations of the micelles are determined by the pairwise radial distribution function, $g(r_{12})=g(R_s)$. Because higher order interactions are neglected, it is consistent to use the pair distribution $g(R_s)$ with the two-particle cumulant theory. The radial distribution gives the probability of finding a pair of space filling micelles a distance R_s apart, relative to that of a completely random distribution at the same number density.

Since the micelles are modeled as hard spheres, $g(R_s)$ is obtained from the solution to the Percus–Yevick (PY) equation. For large separations, $R_s>4R_m$, the algorithm developed by Smith and Henderson[29] was used. For $R_s<4R_m$, the correctional procedure introduced by Verlet and Weis[30] was used. This analytical form for $g(R_s)$ was substituted into Eqs. (2.16) and (2.13c).

III. MONTE CARLO SIMULATION OF EET IN HARD SPHERE MICELLES

The EET dynamics of a system of interacting chromophores is completely determined by the configuration, **K**. In general, **K** is defined by the set $\{\mathbf{r},\omega\}$, where $\mathbf{r}=[r_1,r_2,...,r_N]$ and $\omega=[\omega_1,\omega_2,...,\omega_N]$ are the position and orientation vectors of the N molecules.[23] For the micelle systems considered here, the chromophore orientations are assumed to be random. This has the overall effect of scaling the dynamic Förster transfer distance, R_0, by the orientational parameter, $\gamma^{1/2}$.[11,16,27] The configuration then depends only on the chromophore positions, **r**. The EET dynamics are related to fluorescence depolarization experiments by the probability that an initially excited chromophore is still excited at a later time. This is given by the self part of the Green's function solution to the Pauli master equation

$$\frac{dp_j(\mathbf{K},t)}{dt}=-\frac{p_j(\mathbf{K},t)}{\tau}+\sum_{k=0}^{N}\omega_{jk}[p_k(\mathbf{K},t)-p_j(\mathbf{K},t)], \quad (3.1)$$

where τ is the radiative excited state lifetime and ω_{jk} is the Förster transfer rate between molecules j and k due to the dipolar interaction,

$$\omega_{jk}=\frac{1}{\tau}\left(\frac{\gamma^{1/2}R_0}{r_{jk}}\right)^6. \quad (3.2)$$

Equation (3.1) can be rewritten in matrix form after making the substitution,

$$p'_j(\mathbf{K},t)=p_j(\mathbf{K},t)\exp(-t/\tau). \quad (3.3)$$

Equation (3.1) thus becomes

$$\frac{d\mathbf{p}(\mathbf{K},t)}{dt}=\mathbf{W}\cdot d\mathbf{p}(\mathbf{K},t), \quad (3.4)$$

where **W** is an N by N matrix with elements,

$$W_{jk}=\omega_{jk}-\delta_{jk}\sum_k\omega_{kl} \quad (3.5)$$

and $\mathbf{p}$ is a vector with components $[p_1(\mathbf{K},t), p_2(\mathbf{K},t),...,p_N(\mathbf{K},t)]$. Equation (3.4) has the formal solution,[24]

$$\mathbf{p}(\mathbf{K},t)=\exp(t\mathbf{W})\cdot\mathbf{p}(\mathbf{K},0)=\mathbf{G}(t)\cdot\mathbf{p}(\mathbf{K},0). \tag{3.6}$$

In Eqs. (3.6), $\mathbf{G}(t)$ is the Green's function propagator which represents the conditional probability of finding the excited state probability distribution at time t, $\mathbf{p}(\mathbf{K},t)$, given the initial distribution, $\mathbf{p}(\mathbf{K},0)$. The Green's function elements, $G_{jk}(t)$, are the conditional probabilities of finding an excitation on chromophore j at time t, given the excitation began on chromophore k at time zero. Since the quantity of interest here is the survival probability of initial excitations (the self part of the Green's function), only the diagonal portion of $\mathbf{G}(t)$ contributes to the desired solution. Therefore, $G^s(t)=\mathrm{Tr}[\mathbf{G}(t)]$.

Equation (3.4) is a system of N homogeneous, linear, first order differential equations with constant coefficients. A general solution to this initial value problem can be written as the linear combination[31]

$$\mathbf{p}(\mathbf{K},t)=\sum_{j=1}^{N} c_j\mathbf{v}_j\exp(\lambda_j t), \tag{3.7}$$

where the λ_j's and the $\mathbf{v}_j$'s are the eigenvalues and the corresponding eigenvectors of the matrix $\mathbf{W}$, respectively. The c_j's are determined by the initial condition,

$$\mathbf{p}(\mathbf{K},0)=\sum_{j=1}^{N} c_j\mathbf{v}_j. \tag{3.8}$$

For the case of site-selective excitation in the presence of donor–donor EET, we assume the initial excitation resides completely on one chromophore. Because site numbering is arbitrary, the initial condition is always chosen such that the entire excitation begins on chromophore 1. Then, $\mathbf{p}(\mathbf{K},0)=[1,0,0,...,0]$ and $G^s(\mathbf{K},t)=p_1(\mathbf{K},t)$, the first element of the vector $\mathbf{p}(\mathbf{K},t)$.

Since $\mathbf{W}$ is a symmetric real matrix, in most cases a standard Jacobi method[32] was employed to obtain the eigenvectors and eigenvalues. For the largest systems examined here ($N\approx 60$), the matrix was first tridiagonalized using the Householder reduction method (tred2) followed by the QL algorithm with implicit shifts (tqli).[32] The resulting $\mathbf{v}_j$'s were substituted into Eq. (3.8) to determine the c_j's from the initial condition. Equation (3.7) was then evaluated to give $G^s(\mathbf{K},t)$ for the particular configuration $\mathbf{K}$. The process was repeated for many configurations to obtain the average $\langle G^s(t)\rangle$.

A. Generation of configurations: Chromophores on the surfaces of spheres

A reasonable starting point for the description of chromophore–micelle systems is the hard sphere model.[33] In the calculations presented below, viable chromophore configurations were generated with the probe positions randomly located on the surfaces of hard spheres. We focus on two types of related situations: (i) Chromophores randomly distributed on the surface of a single, isolated sphere is a model for intramicelle EET. (ii) Chromophores randomly distributed on the surfaces of many hard spheres (which pack in space as in a hard sphere fluid) is a model for the combined processes associated with intra- and intermicelle EET. Type (i) calculations only involve an average over chromophore configurations. This is called Monte Carlo integration since random numbers are used to sample the coordinate space of the chromophores. An important distinction between this and type (ii) calculations is the effect of the micelle excluded volume. The hard sphere interaction leads to complicated micelle solution structure that requires an involved, although well established, acceptance–rejection simulation technique. A type (ii) calculation is, in fact, an integration over chromophore configuration space which depends on the *simulated* structure of the hard sphere micelle system. After a brief description of the random number generator, we begin with the simplest case (i), and then proceed to multiple sphere systems (ii) with various packing densities.

1. Random number generator

All Monte Carlo methods employ the use of a random number generator (rng) to sample the ranges of the functions of interest. We chose the algorithm by Marsaglia and Zaman[34] for its extremely large period ($\sim 10^8$) and its ability to satisfy important statistical tests. This algorithm required 24 input seed numbers which were obtained from another rng (Ref. 35) with a shorter period. At the beginning of all calculations, 10 000 initial calls to the rng were made to eliminate correlations with the original seed number values.

2. Monte Carlo integration

Consider a single sphere with radius R_m centered at the origin (Fig. 1). We wish to choose chromophore coordinates that are randomly located on the sphere's surface. In spherical coordinates, each chromophore is specified by the vector components $[r_i, \theta_i, \varphi_i]$. Since all the probe molecules lie on the sphere's surface, the radial component, r_i, is equal to the micelle radius, R_m. Each chromophore then has two independent degrees of freedom which must be specified. The polar angle, θ, can have values in the interval $[0,\pi]$; the azimuthal angle, φ, in the interval $[0,2\pi]$. As illustrated in Fig. 2(a), a purely random sampling in the range of θ would incorrectly result in high chromophore densities at the sphere's poles. The choice of θ must therefore be weighted by the probability of finding a chromophore with this component. This is given by the normalized distribution,

$$P(\theta)=\tfrac{1}{2}\sin\theta. \tag{3.9}$$

It is shown in Appendix C that the correctly weighted distribution in θ is obtained from the function [Fig. 2(b)]

$$\theta=\mathrm{acos}(1-2\cdot F), \tag{3.10}$$

where F is a random number in the interval $[0,1]$. The distribution in φ, on the other hand, is obtained from a uniform sampling of its range

$$\varphi=2\pi\cdot F. \tag{3.11}$$

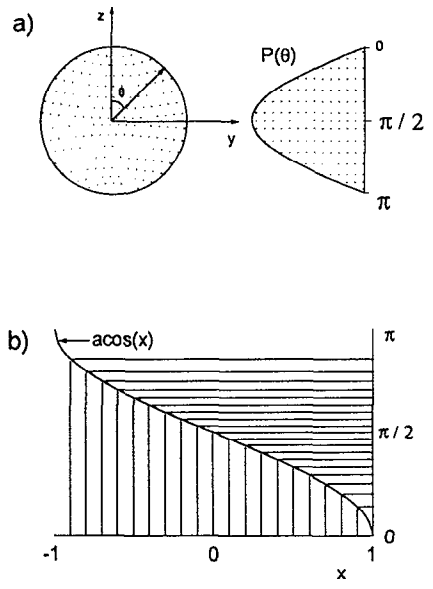

FIG. 2. (a) Schematic representation of the point density on a spherical surface as a function of the polar angle, θ. The density of points follows the form of the normalized function, Eq. (3.9). (b) The $\cos^{-1}$ function is used to map a uniformly chosen number into the desired distribution (see Appendix C).

For a micelle that contains N chromophores, $2N$ calls to a random number generator are required. After transforming from polar to Cartesian coordinates, the $N(N-1)/2$ separation vectors are calculated and substituted into Eqs. (3.2) and (3.5). This procedure is repeated until the "configuration space" has been sufficiently sampled and $\langle G^s(t)\rangle$ does not change with additional contributions to the configurational integral. Typically, 10 000 configurations were sufficient for this purpose.

3. Monte Carlo simulation of a hard sphere micelle system

In order to generate viable chromophore configurations for multiple hard sphere systems, it is necessary to employ standard MC simulation methods to obtain the sphere coordinates.[22] A brief description of the procedure follows.

A cubic box of length L has its center at the origin. For a given packing density, η, the number of spheres (n) in the box is determined according to

$$n=\eta\frac{3}{4\pi}\left(\frac{L}{R_m}\right)^3. \tag{3.12}$$

For example, $L=500$ Å, $R_m=37$ Å, and $\eta=20\%$ corresponds to 117 spheres. Initially, the sphere configuration was generated by randomly choosing the $3n$ orthogonal coordinates of the n sphere centers

$$r_{\alpha i}=(1-2F)\cdot(L/2-R_m), \tag{3.13}$$

where α collectively represents the three orthogonal Cartesian components of the position vectors. To prevent spheres from overlapping, the distances between sphere centers were calculated upon the generation of a new position. A new sphere that overlapped with any other was discarded and a new set of coordinates were chosen for this sphere. Depending on the packing density, this often required a substantial number of trials before an initial nonoverlapping system of spheres was achieved.

Since the initial configuration is randomly chosen, the distribution of pairwise distances between spheres fall off exponentially (as in a Poisson distribution). These random configurations were then "equilibrated" according to the Metropolis method. The application of periodic boundary conditions in conjunction with the minimum image convention are described in some detail in Appendix D. Each "equilibration step" consisted of the random selection of a sphere and its translation within a cube of adjustable size. Steps that resulted in sphere collisions were rejected and the previous configuration was recovered. The cube size was adjusted every 50 MC steps so that an average of half of the trials were accepted. Typically, 10 000 initial configurations, each with 1000 equilibration steps, were used to obtain a uniform sampling of viable hard sphere configurations. This was confirmed by calculating the radial pair distribution function, $g(r)$, from the simulated sphere separations.[22]

For each hard sphere configuration, a corresponding system of N chromophores was generated for an N particle, many micelle EET calculation. Chromophore coordinates were generated on the individual spherical surfaces as described above for the single sphere case. The number of chromophores assigned to any particular sphere was randomly selected from a weighted function determined by a Poisson distribution about the mean value, ν (see Appendix C). Using the minimum image convention, the set of spherical polar chromophore coordinates was transformed into $\nu\cdot n$ absolute sets of Cartesian coordinates with the origin placed at the position of chromophore 1 (Fig. 3).

The total number of chromophores included in the EET calculations were limited by employing a spherical cutoff procedure. As illustrated in Fig. 3, a spherical shell with radius R_{co} was constructed with its center at the position of chromophore 1. Hard spheres with centers that lay outside the region enclosed by the spherical shell were ignored. Only chromophores belonging to spheres that lay inside the shell were considered part of the N particle system. EET calculations were performed for several cutoff distances. On comparison, these proved to be invariant for $R_{co}\geqslant 3R_0$.

IV. RESULTS AND DISCUSSION

In order to achieve a meaningful comparison between the MC results and those of the analytical theory for DD systems, it is necessary to establish some confidence in the numerical procedures. The four different types of physical situations described here are DT and DD transport in the isolated micelle (hard sphere) and DT and DD transport for many interacting micelles (many hard spheres). Each system will be examined separately in increasing order of complexity.

All the calculations presented below used experimentally realizable values for the sphere radius and the static

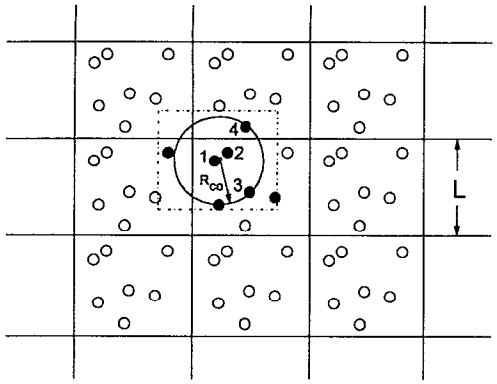

FIG. 3. Schematic representation of the application of periodic boundary conditions and the minimum image convention applied to EET calculations of chromophores on the surfaces of hard sphere micelles. During the simulation, the periodic boundary condition helps to conserve the number of spheres in the box and prevents the appearance of anomalous edge effects. The dotted lines are the boundaries of the minimum image box centered at the position of the initially excited chromophore. Only minimum image hard spheres (shaded) contain chromophores which are considered in the EET calculation. The number of chromophores is further reduced by using the spherical cutoff, R_{co}. The hard spheres whose centers lie inside this shell (labeled 1 through 4) are included in the final calculations.

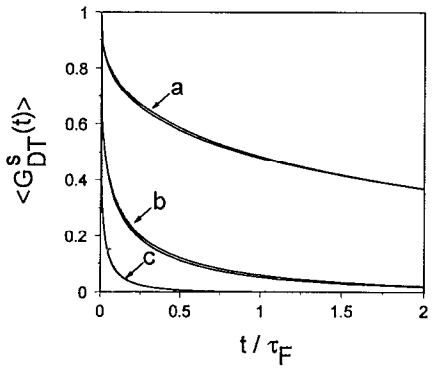

FIG. 4. Comparison of MC calculations and analytical theory [Eq. (2.5)] for DT EET among chromophores randomly distributed on the surface of an isolated spherical surface. The total number of chromophores on the sphere (one donor plus $N-1$ traps) are (a) 2, (b) 5, and (c) 10.

Förster transfer distance, $R_m=37$ Å and $\gamma^{1/2}R_0=47.39$ Å. For the DD systems, additional values for these parameters were examined to illustrate their effect. For simplicity, the DD and DT critical transfer distances were assumed to be the same.

A. Single sphere systems

1. DT transport

MC calculations were carried out for one donor and $N-1$ traps distributed on a single spherical surface. The calculations were performed by generating the chromophore configurations as described in Sec. III A 2 and Appendix C. The set of donor–trap separations was then substituted into

$$G^s(t)=\exp\left(-\sum_{i=2}^{N}\omega(\mathbf{r}_{1i})t\right), \tag{4.1}$$

where $\omega(\mathbf{r}_{1i})$ is defined by Eq. (2.2).[27] Provided the chromophore coordinates are sampled correctly from the spherical distribution, repeating this procedure many times, and averaging the result effectively evaluates the configurational integrals in Eq. (2.1). The exact analytical expression is given by Eq. (2.5). Figure 4 shows comparisons of the MC results and Eq. (2.5) for three different values of N. All the decays go to zero at long time because the initial donor excitation is eventually depleted by transfer to trap chromophores. The examples shown are for (a) one donor and one trap, (b) one donor and four traps, and (c) one donor and nine traps. In all three cases, the MC calculation was performed with 1000 iterations.

While not perfect, the excellent agreement between the analytical and MC results indicates that the single sphere configuration space is effectively sampled by the MC method. This information is necessary for the analysis of the more complicated systems below.

2. DD transport

MC calculations for N donors on a single sphere were carried out according to the procedures outlined in Sec. III. The chromophore configurations were chosen just as for the single sphere DT problem. Since the maximum number of chromophores considered was 15, the Jacobi method was sufficient to perform the necessary matrix diagonalizations. At the beginning of each iteration, the total number of chromophores on the sphere was chosen from a weighted function determined by a Poisson distribution with a mean value of ν (Appendix C). The resulting configurational average, $\langle G^s(t)\rangle$, represents the observable DD EET dynamics of an ensemble of spheres with a Poisson average of ν probes per micelle. Again, 1000 iterations were sufficient to achieve a convergent result.

Figures 5(a) and 5(b) show comparisons of the MC single sphere DD results with those given by the cumulant theory. Figure 5(a) is for $\nu=3$, Fig. 5(b) is for $\nu=5$. The comparisons are made over the range of Q between 0.1 and 1.3. It was discussed in Sec. II B 2 that Eq. (2.7) is only accurate for small N or small Q. The analytical results shown in Figs. 5(a) and 5(b) are Poisson averaged Padé approximants constructed from Eq. (2.7). The use of these functions are explained in Appendix B. These individual functions were favorably compared with MC calculations for the relevant values of N and Q.

Unlike the single sphere DT results, the decays do not asymptotically approach zero. The residual survival probability is a function of the number of chromophores in the finite volume. This asymptotic value is given by

$$G^s(t)=\left(\frac{1}{1-e^{-\nu}}\right)\sum_{N=1}^{\infty}\frac{e^{-\nu}\nu^N}{N!}\left(\frac{1}{N}\right), \tag{4.2}$$

which is the renormalized Poisson average (for $N\neq 0$) of the asymptotic limit of $G^s(t\to\infty;N)=1/N$. Equation (4.2) converges to

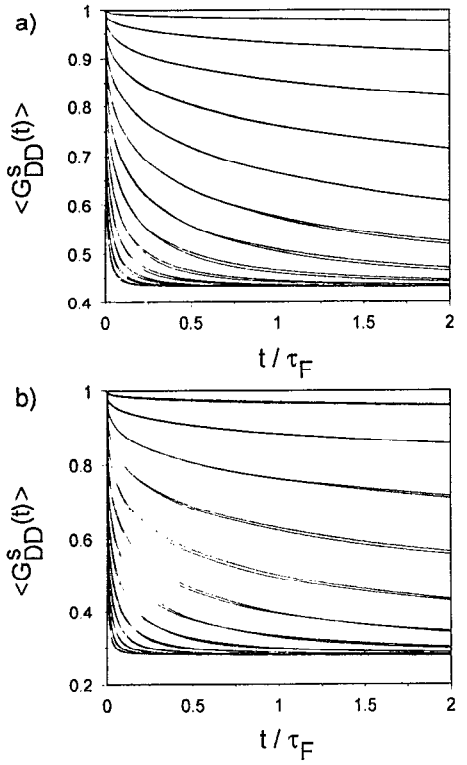

FIG. 5. Comparison of MC calculations and first order cumulant theory for DD EET among chromophores randomly distributed on the surface of an isolated spherical surface. The curves described by the analytical theory are given by Poisson averages of Eqs. (B1)–(B5) as described in Appendix B. The two sets of comparisons correspond to different mean occupation numbers; (a) $\nu=5.0$ and (b) $\nu=3.0$. In both figures, the different sets of curves represent different values of the quotient $Q=R_0/2R_m$. The values of Q shown are 0.1, 0.2, 0.3, 0.4, 0.5, 0.6, 0.7, 0.8, 1.0, 1.1, 1.2, and 1.3.

$$\frac{-\gamma+Ei(\nu)-\ln(\nu)}{e^{\nu}[1-e^{-\nu}]}, \tag{4.3}$$

where

$$Ei(\nu)=-\int_{-\nu}^{\infty}\frac{e^{-t}}{t}dt$$

is the exponential integral function, and γ is Euler's constant, 0.577 216. For $\nu=3$ and 5, Eq. (4.3) is 0.433 and 0.258, respectively, in agreement with the asymptotic values shown in Figs. 5(a) and 5(b).

The agreement between the analytical and MC results is excellent. This indicates that Eqs. (C1)–(C5) accurately represent the hard sphere model for DD transport and that the MC procedure discussed in Appendix D reproduces the Poisson average used in the analytical theory.

B. Many sphere systems

1. Hard sphere solution structure

The EET calculations for systems of interacting spheres depend, at the first level, on the sphere configurations. The simplest way to characterize the hard sphere structure is with the pair distribution, $g(r_{12})=g(r)$

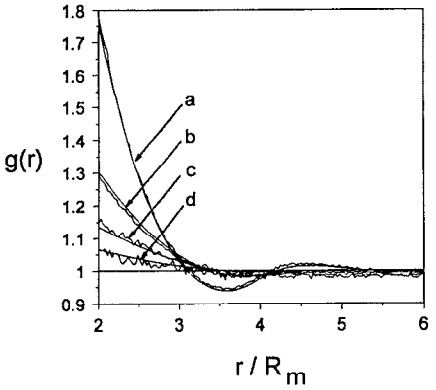

FIG. 6. Comparison of radial pair distribution functions obtained from the MC simulations and solutions to the Percus–Yevick equation. The packing densities [Eq. (3.12)] are (a) 20%, (b) 10%, (c) 5%, and (d) 2.5%.

$$g(r)=\frac{V}{N^2}\left\langle\sum_i\sum_{j\neq i}\delta(\mathbf{r}-\mathbf{r}_{ij})\right\rangle. \tag{4.4}$$

As described in Sec. III A 3, during an MC simulation a viable hard sphere configuration is reached after ~1000 equilibration steps. The radial distribution function is constructed by building a histogram of the occurrence of pairwise separations.[22] The procedure is reiterated (typically, 10 000 times) during the course of the calculation, until an ensemble average is achieved.

In Fig. 6, the radial distribution function obtained from MC simulation is compared to the corresponding solutions of the Percus–Yevick equation. In all cases, the box length, $L=500$ Å and the sphere radius, $R_m=37$ Å. The four different packing densities shown are for (a) 20%, (b) 10%, (c) 5%, and (d) 2.5%. This corresponds to (a) 117, (b) 58, (c) 29, and (d) 14 spheres in the box. Although the MC and PY functions are not identical, the very close agreement indicates that the hard sphere configurations are properly emulated. For subsequent comparisons between MC and analytical EET calculations, the PY solutions have been inserted into the analytical theories [see Eqs. (2.13b) and (2.17)].

2. DT systems

Chromophore configurations were generated from the simulated hard sphere distributions as described in Sec. III A 3 and Appendix D with $\nu=5.0$. It is important to note that the number of chromophores necessary for the EET calculation, and hence the number of hard sphere surfaces which they lie on, is signifacantly smaller than the total number of hard spheres (n_{box}) initially required for the equilibration procedure. The total number of chromophores (N) were limited by using the spherical cutoff, $R_{co}=3R_0$, illustrated in Fig. 3. This means, for example, that the number of hard spheres contained in the spherical shell (n_{co}) with packing density, $\eta=20\%$, is $(V_{co}/V_{Box})\cdot n_{box}=0.096\times 117=11.2$. Then, the number of chromophore involved in the EET calculation is $\nu\cdot n_{co}=5\times 11.2=56$. The resulting $N-1$ donor–trap separations

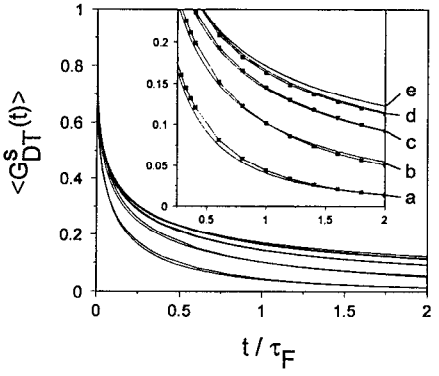

FIG. 7. Comparison of MC calculations and analytical theory (Sec. II B 1) for DT EET among chromophores randomly distributed on the surfaces of many interacting spheres. The analytical theory is shown in the inset with square markers. The decay of $\langle G^s_{DT}(t)\rangle$ is shown as a function of packing density, η: (a) 20%, (b) 10%, (c) 5%, (d) 2.5%, and (e) isolated micelles.

were substituted into Eq. (4.1) to obtain $G^s(t)$ for the N-body system. The configurational average, $\langle G^s(t)\rangle$, was obtained from $\sim 10\,000$ reiterations of the entire procedure, beginning with the regeneration of a completely new hard sphere configuration.

Figure 7 shows comparisons of the MC simulations and the analytical DT theory outlined in Sec. II B 1. A blow up of the long time behavior is shown in the inset. Different sphere packing densities are indicated in the inset as (a) 20%, (b) 10%, (c) 5%, (d) 2.5%, and (e) isolated spheres. The analytical theory is shown with square markers. Although the agreement is not perfect, it is extremely good. The slight differences are attributed to inaccurate representations of the chromophore configurations, either by numerical inaccuracies of the analytical formulation or by the MC simulation. These differences, however, are relatively insignificant since the overall functionality and magnitude of the decays are the same. This favorable comparison is a direct test of the analytical procedure employed by the EC method. The agreement shown in Fig. 7 suggests that the analytical calculation of $\langle G^s_{off}(t;R_s)\rangle$ carried out in Eqs. (2.14), is essentially correct. In the present DT problem, this function is exactly related to $\langle G^s(t)\rangle$ through Eqs. (2.13b) and (2.10). However, for the analogous DD problem, Eq. (2.10) is an approximation based on the two-particle cumulant and EC methods. Since the configurational integrals used to evaluate $\langle G^s_{off}(t)\rangle$ in the DD problem are very similar to the ones used for this DT problem, any inaccuracy in the EC method must be due to a failure of the two-particle approximation and not to an incorrect calculation of the configurational integrals.

3. DD systems

The donor chromophore configurations were generated as in the DT many sphere system with $\nu=5.0$. Again, the total number of chromophores were limited using a spherical cutoff of $3R_0$. The highest sphere packing density ($\eta=20\%$) corresponds to $N\approx 60$ chromophores. For most configurations, the W matrix was first tridiagonalized using

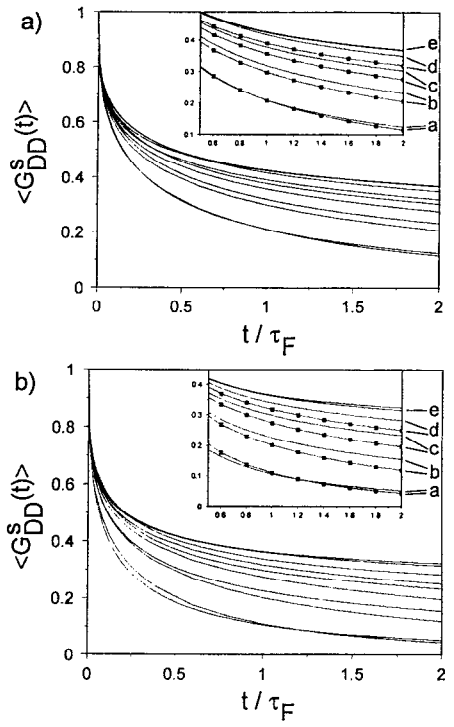

FIG. 8. Comparison of MC calculations and first order cumulant theory (Sec. II B 2) for DD EET among chromophores randomly distributed on the surfaces of many interacting spheres. The analytical theory is shown in the insets with square markers. Figure 8(a) corresponds to the micelle radius $R_m=42$ Å. Figure 8(b) is for $R_m=37$ Å. The packing densities are labeled as in Fig. 7.

the Householder reduction method, followed by the QL algorithm with implicit shifts. This is much faster than the Jacobi method. However, some configurations were found to be non-convergent using the Householder method, and in these cases the Jacobi method was used. For most conditions, the final solution was checked by comparison with calculations that only used the Jacobi routine.

Figures 8(a) and 8(b) shows comparisons of the DD MC calculations with the first order cumulant approximation. In Fig. 8(a), $R_m=42$ Å, in Fig. 8(b), $R_m=37$ Å. The former radius value was chosen because it is the effective radius of gyration reported from light scattering measurements of triton X-100 micelles.[15] The latter value is the one most consistent with previous experiments of EET in isolated triton X-100 micelle systems.[16,15] The different packing densities are labeled in the insets as (a) 20%, (b) 10%, (c) 5%, (d) 2.5%, and (e) isolated spheres. The analytical theory is shown with square markers. Although the agreement is not perfect, it is reasonably good. For both micelle radii, the comparisons appear to be most similar at the highest density, $\eta=20\%$. The agreement becomes progressively worse as the density decreases, although the magnitude and form of the decays are basically the same.

The cumulant appears to overestimate the decay of $\langle G^s(t)\rangle$ at all densities, although there is a crossover for $\eta=20\%$. The reason for this may be understood in terms of an argument based on analogy. It has been previously shown[36] that the first order cumulant approximation is in

essentially perfect agreement with more accurate representations of $\langle G^s(t)\rangle$ for infinite three dimensional isotropic distributions of chromophores. It is reasonable to expect the chromophore distributions for the $\eta=20\%$ systems to resemble an infinite isotropic system more than those at lower densities. Generally, the cumulant is known to decay too quickly for finite volume systems [see Eq. (2.8)]. However, as the sphere density increases towards 20%, the spatial fluctuations in the chromophore density become small and the interchromophore distances begin to resemble those found in a random, infinite isotropic system. If the micelle concentration is increased even further, the micelle excluded volume will eventually cause the spatial fluctuations in the chromophore density to increase again, because on the average chromophores on neighboring micelles will be closer to a given site than chromophores on the same micelle.

In order to comment on the importance of the discrepancies found in the above analysis, it is necessary to determine the degree of accuracy required of the EC method for its useful incorporation into meaningful experimental measurements. In the following subsection, we compare the theoretical and simulation results together with experimental data.

C. Experimental investigations

Previously, experiments were carried out on octadecylrhodamine B(ODRB) in aqueous triton X-100 micelles.[16] In this study, time resolved fluorescence depolarization measurements of the ODRB probes were made as a function of the micelle volume fraction, while the ratio of ODRB molecules to micelles ($\nu=5.0$) was held constant. The aliphatic portion of the ODRB molecule causes essentially all of the probes to be solubilized in the micelles with the charged chromophoric head group positioned near the water/micelle interface. The triton X-100 micelles are believed to form approximately monodisperse spherical colloidal aggregates for the range of concentrations studied.[37]

Time resolved polarized fluorescence measurements are related to $\langle G^s(t)\rangle$ through the time dependent fluorescence anisotropy

$$r(t)=\frac{I_{\parallel}(t)-I_{\perp}(t)}{I_{\parallel}(t)+2I_{\perp}(t)} \tag{4.5}$$

$r(t)$ contains all sources of depolarization. For a solution characterized by the micelle volume fraction η, and the mean number of probes per micelle ν, the time dependent anisotropy is given by

$$r(t,\nu,\eta)=\langle\Phi(t)\langle G^s(t,\nu,\eta)\rangle\rangle. \tag{4.6}$$

Here $\Phi(t)$ contains processes besides energy transport which contribute to the depolarization. The most important of these is molecular reorientation which, in this analysis, is assumed to be much slower than the energy transport. The outside brackets in Eq. (4.6) indicate a configurational average that includes correlations between $\Phi(t)$ and the energy transport. For slow chromophore rotation, the difference in time scales dictates that the correlations are insignificant and that excitation transport is independent of the molecular rotation. Thus Eq. (4.6) can be written as

$$r(t,\nu,\eta)=r_{\rm rot}(t)\cdot\langle G^s(t,\nu,\eta)\rangle, \tag{4.7}$$

where $r_{\rm rot}(t)$ is the rotational contribution to the anisotropy.

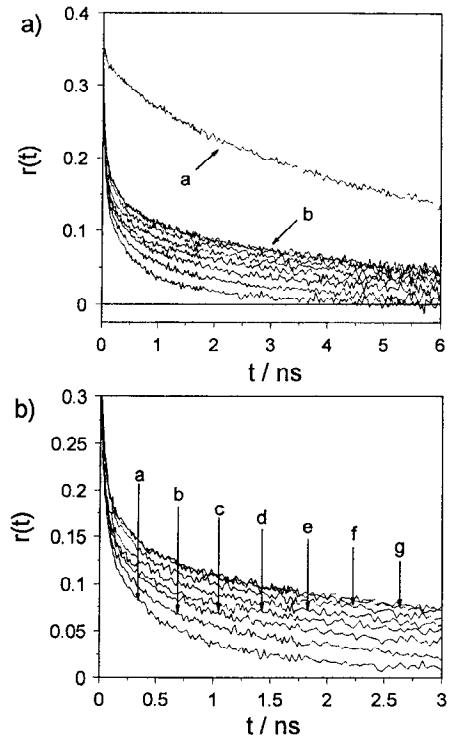

FIG. 9. Time dependent fluorescence anisotropy data from octadecylrhodamine B (ODRB)/triton X-100/water systems. The data is reproduced from Ref. 16. In (a) the rotational contribution to the anisotropy (a) is compared to decays which contain both rotational and EET contributions. For all of the EET samples, the mean occupation number, $\nu=5.0$. The packing densities are labeled in (b): (a) 20%, (b) 15%, (c) 10%, (d) 5%, (e) 2.5%, (f) 1.25%, (g) 0.625%, and 0.313%.

Figure 9(a) shows fluorescence anisotropy data originally presented in Ref. 16. The lifetime of the ODRB probe was reported as $\tau_F=2.69$ ns. The decay labeled (a) represents a sample which contained fewer than 1 ODRB molecule for every 15 micelles ($\nu=0.06$). This was fit to a biexponential function to model the rotational component of the anisotropy

$$r_{\rm rot}(t)=0.0363\exp(-t/0.388\ \text{ns})+0.2987\exp(-t/6.999\ \text{ns}). \tag{4.8}$$

The decays labeled (b) represent samples which have $\nu=5.0$ with increasing micelle density. The apparently large difference in magnitude between the rotational and EET decays suggests that Eq. (4.7) is a reasonably good approximation.

The effect of micelle density on $r(t)$ is more clearly shown in Fig. 9(b) with an expanded time scale. The different micelle concentrations are labeled as (a) 20%, (b) 15%, (c) 10%, (d) 5%, (e) 2.5%, (f) 1.25%, and (g)

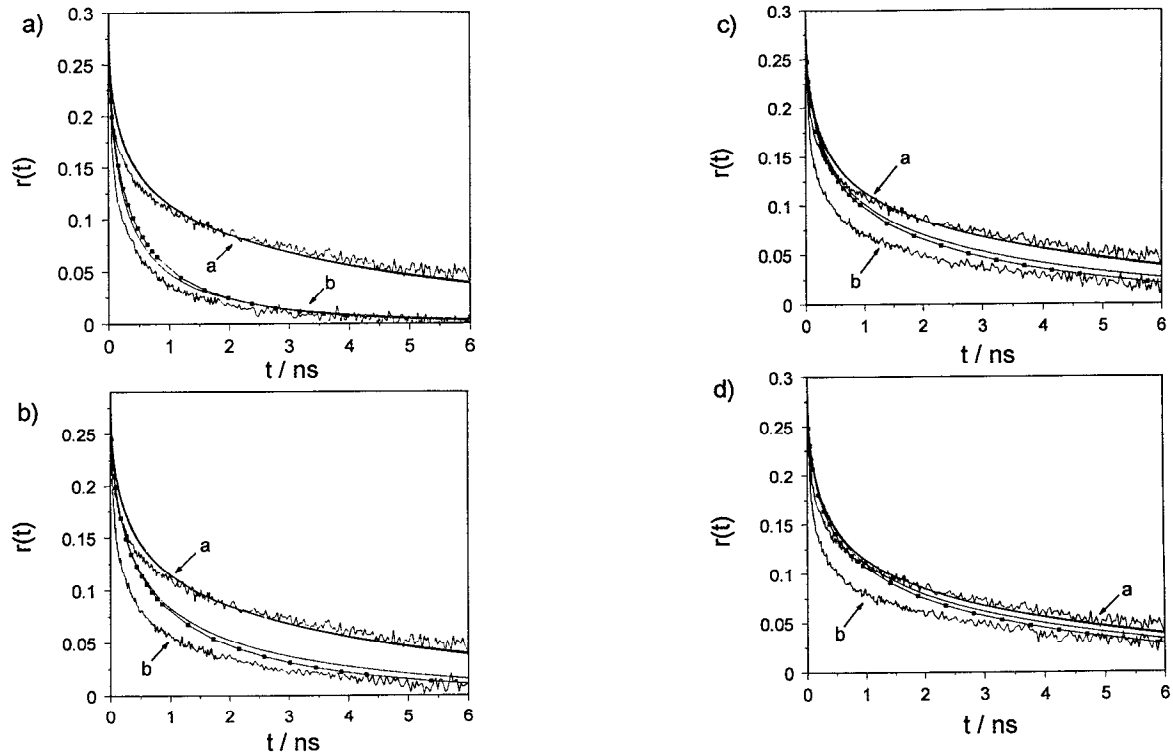

FIG. 10. Comparison of MC calculations and first order cumulant theory for many sphere DD EET and experimental data from Ref. 2. In (a) through (d), the decays due to intramicelle EET are labeled (a) and those due to intermicelle EET are labeled (b). The different packing densities are (a) 20%, (b) 10%, (c) 5%, and (d) 2.5%.

0.625% and 0.313%. The decay rates all decrease monotonically with decreasing micelle density, corresponding to a decrease in intermicelle EET. The two decays labeled (g) are identical indicating that all of the energy transport observed in these samples, which differ in micelle density by a factor of 2, are due to intramicelle EET.

Using Eqs. (4.7) and (4.8), both MC simulations and the analytical results for the DD many sphere systems were converted to theoretical anisotropies. For these calculations the micelle radius, $R_m=37$ Å, consistent with previous studies of the ODRB/triton X-100/water system.[16,15] These are compared to the experimental data in Figs. 10(a)–10(d).

For all these figures, the set of decays labeled (a) represent the fluorescence anisotropy due to intramicelle EET. The analytical theory and the MC simulation is almost identical for these decays. It has been previously suggested that the disagreement between the experimental data and theory at short time is due to a non-Poisson chromophore distribution. The effect of chromophore density on the intramicelle EET observable was examined in detail in Ref. 16. It was shown that a skewed Poisson distribution resulting from probe–probe interactions could account for these intramicelle disagreements at higher probe concentrations.

The set of decays labeled (b) are comparisons of the MC simulations, analytical theory, and experimental data for the four different micelle densities. Figure 10(a) shows $\eta=20\%$; Fig. 10(b), 10%; Fig. 10(c), 5%; and Fig. 10(d), 2.5%. The differences between the analytical theory and the simulations are relatively small compared to the disagreement between theory and data. The theoretical anisotropies decay too slowly for all the concentrations. However, the highest concentration ($\eta=20\%$) appears to come closest to the theoretical predictions. This agreement becomes worse as the micelle concentration is decreased. It is apparent from Figs. 10(a)–10(d) that the analytic theory is accurate enough to use as a modeling tool for the analysis of this data.

The proven reliability of the cumulant for static chromophore configurations makes it possible to study the effect of chromophore motion on EET in dynamical systems. The octadecylrhodamine B/triton X-100/water systems discussed in this work exhibit dynamical properties,[25] although their influence on the fluorescence depolarization observables are not completely understood. The most important effect is the translational diffusion of the chromophores on the micelle surface. This makes the chromopohore positions time dependent. Chromophore translation may play an important role in the disagreement between theory and data shown in Figs. 10(a)–10(d). Therefore, further analysis of these systems will require an assessment of the importance of chromophore translational diffusion on the energy transport.

The second potential source of the disagreement is due to an inappropriate model of the chromophore distributions, here assumed to be distributed as hard spheres. For example, an attractive micelle–micelle interaction potential could have the effect of creating micelle pairs (perturbed

radial distributions shifted toward shorter distances). Such a situation would lead to faster depolarization decays than the hard sphere model predicts. The effect of pairing would be most pronounced at low concentrations where shifting the distances between micelles toward closer spacing would be a significant change from the distances that would be present for a hard sphere distribution. At higher concentrations, the effect would be masked somewhat by the small intermicelle spacings that would be encountered even for a hard sphere distribution. At all concentrations, the short time behavior (corresponding to fast, short distance transfer events) would be most significantly effected. This scenario is consistent with the observations and may be responsible for the differences between the experiments and theory.

V. CONCLUDING REMARKS

The analysis presented above is the first detailed examination of the validity of the first order cumulant approximation for the description of interacting clusters of chromophores. The results indicate that the cumulant theory accurately predicts the energy transport dynamics based on the configurational models depicted here. The most important implication is that the first order cumulant approach, an analytically tractable method, is a suitable tool for the structure elucidation of systems that involve complicated probe distributions.

The advantage of the cumulant method over MC procedures is its relative ease of use. The configurational integrals often have analytical expressions or are readily evaluated using standard numerical quadrature. In contrast, MC methods often require substantial computation time and must be carefully scrutinized to insure proper sampling of the configurational space. For the case of intramicelle DD EET, the Padé corrected cumulant, Eqs. (B1)–(B5), accurately describe the transport dynamics for a broad range of chromophore numbers and sphere radii. The effect of probe–probe interactions on the micelle occupancy[16] can be readily examined using these functions. Similarly, intermicelle DD EET can be accurately described using the EC method. More realistic forms for the radial distribution function can then be easily substituted into Eq. (2.16) to obtain self-consistent information concerning micelle–micelle interactions.

One possible application of the EC approach is towards understanding nanophase separated domains in two-component polymer blends. Excitation transport experiments on concentrated mixtures of chromophore tagged polymer chains in untagged polymer hosts have recently provided information on intermolecular polymer chain structure in single-component materials with angstrom resolution.[17] Extension of the EC method with appropriate perturbation theories will provide information on the structure and dynamics of nanophase separation in polymeric materials.[38] Similar work can be used to obtain correlation hole information in block copolymer systems. An accurate description of EET in the presence of dynamical disorder may be applied to related problems such as structure elucidation and dynamics in biomolecular systems.

ACKNOWLEDGMENTS

We would like to thank Professor Alice Gast, Professor Harald Kauffman, and Dr. Walter Kobb for helpful discussions. We would also like to thank Professor Gast and David Marr for providing us with the computer code used to perform the PY calculations. K.U.F. would like to acknowledge support from the German National Scholarship Foundation. This work was supported by the Department of Energy, Office of Basic Energy Sciences (DE-FG03-84ER13251). Additional support was provided by the Stanford Center for Materials Research Polymer Thrust Program and an NSF departmental instrumentation Grant (No. CHE 88-21737) which is responsible for the computer equipment used in the calculations.

APPENDIX A: DERIVATION OF DT EQUATION FOR A SINGLE SPHERE

Consider a sphere of radius R_m, centered at the origin as shown in Fig. 1. From Eq. (2.4),

$$\langle G^s(t)\rangle = \left(\int_{\mathbf{r}_2} P(\mathbf{r}_2)\exp[-\omega(\mathbf{r}'_{12})t]d\mathbf{r}_2 \right)^{N-1}. \quad \text{(A1)}$$

For a hard sphere system,

$$P(\mathbf{r}_2) = \frac{\delta[r_2 - R_m]}{4\pi R_m^2}$$

and

$$d\mathbf{r}_2 = r_2^2 \sin\theta_2\, dr_2\, d\theta_2\, d\varphi_2, \quad \text{(A2)}$$

where $\delta[x]$ is the Dirac delta function. It then follows,

$$\langle G^s(t)\rangle = \left(\frac{1}{4\pi R_m^2} \int_{r_2} \int_{\theta_2} \int_{\varphi_2} \exp[-\omega(\mathbf{r}'_{12})t] \times \delta[r_2 - R_m] r_2^2 \sin\theta_2\, dr_2\, d\theta_2\, d\varphi_2\, dr_2 \right)^{N-1}. \quad \text{(A3)}$$

The integrals over r_2 and φ_2 can be evaluated immediately to give,

$$\langle G^s(t)\rangle = \left(\frac{1}{2} \int_{\theta_2} \exp[-\omega(\mathbf{r}'_{12})t] \sin\theta_2\, d\theta_2 \right)^{N-1}. \quad \text{(A4)}$$

The following geometrical relationships can be derived from Fig. 1

$$r'_{12} = 2R_m \cos\theta'_{12}, \quad \text{(A5a)}$$

$$r_2 \sin\theta_2 = r'_{12} \sin\theta'_{12} \Rightarrow, \quad \text{(A5b)}$$

$$R_m \sin\theta_2 = 2R_m \cos\theta'_{12} \sin\theta'_{12} \Rightarrow \sin\theta_2 = 2\cos\theta'_{12} \sin\theta'_{12}, \quad \text{(A5c)}$$

$$d\theta_2 = 2\, d\theta'_{12}. \quad \text{(A5d)}$$

With the above relationships and using Eq. (2.2) for $\omega(\mathbf{r}'_{12})$, Eq. (A4) becomes

$$\langle G^s(t)\rangle = \left(2\int_{\theta'_{12}} \exp[-(R_0/2R_m)^6(1/\cos\theta'_{12})^6(t/\tau_F)] \times \cos\theta'_{12}\sin\theta'_{12}\,d\theta'_{12}\right)^{N-1}. \quad \text{(A6)}$$

Standard methods of integral calculus lead from Eq. (A6) to the analytical solution, Eq. (2.5).

APPENDIX B: PADÉ APPROXIMANTS FOR DD EET ON A SINGLE SPHERICAL SURFACE

Padé Approximants were constructed for Eq. (2.7). They depend on the number of chromophores per micelle and the value of $Q=R_0/2R_m$. These analytical functions reproduce MC results when used with the following constraints [see Figs. 5(a) and 5(b)]:

N	Q	Equation
2	[0.0, 0.6],	(B1)
	(0.6, 1.0),	(B3)
	[1.0, 1.3],	(B4)
3	[0.0, 0.6],	(B1)
	(0.6, 1.3],	(B4)
4–6	[0.0, 0.3],	(B2)
	(0.3, 1.3],	(B4)
7–15	[0.0, 0.3],	(B2)
	(0.3, 0.5],	(B4)
	(0.5, 1.3].	(B5)

$$\ln G^s(t,N) = \frac{((N-1)/2)[-x\Gamma(\frac{2}{3}) + \ln(1/N)x^2/2\Gamma(\frac{2}{3})]}{1+((N-1)/2)[x^2/2\Gamma(\frac{2}{3})]}, \quad \text{(B1)}$$

$$\ln G^s(t,N) = \frac{((N-1)/2)[-x\Gamma(\frac{2}{3})]}{1+((N-1)/2)[x^2/2\Gamma(\frac{2}{3})]}, \quad \text{(B2)}$$

$$\ln G^s(t,N) = \frac{((N-1)/2)\left[\frac{x^3}{2} - x\Gamma(\frac{2}{3}) - \frac{2x^2\Gamma(\frac{2}{3})^2}{5} + 3\ln(1/N)x^6\right]}{1+((N-1)/2)\left[\frac{x^3}{5} + \frac{2x\Gamma(\frac{2}{3})}{5} + 3x^6\right]} \quad \text{(B3)}$$

$$\ln G^s(t,N) = \frac{((N-1)/2)\left[-x\Gamma(\frac{2}{3}) + \frac{23x^3}{48} - 5\Gamma(\frac{2}{3})x^4 - \ln(1/N)\left(\frac{1}{96\Gamma(\frac{2}{3})}+5\right)x^5\right]}{1+((N-1)/2)\left[\frac{x^2}{48\Gamma(\frac{2}{3})} + \frac{5x^3}{24} + \left(\frac{1}{240\Gamma(\frac{2}{3})}+5\right)x^5\right]}, \quad \text{(B4)}$$

$$\ln G^s(t,N) = \left(\frac{N-1}{2}\right)\left[\frac{22523}{42875}x^3 + \frac{6037}{94325}x^6 - \frac{2171x^5}{171500\Gamma(\frac{2}{3})} + \frac{19539x^8}{2358125\Gamma(\frac{2}{3})} - x\Gamma(\frac{2}{3}) - \frac{86x^4\Gamma(\frac{2}{3})}{245} - \frac{19x^7\Gamma(\frac{2}{3})}{539} + 8\ln\left(\frac{1}{N}\right)x^8\right] \Bigg/ 1+\left(\frac{N-1}{2}\right)\left[\frac{86x^3}{245} + \frac{19x^6}{539} - \frac{2171x^2}{85750\Gamma(\frac{2}{3})} + \frac{2171x^5}{188650\Gamma(\frac{2}{3})} + \frac{2171x^8}{646800\Gamma(\frac{2}{3})} + 8x^8\right]. \quad \text{(B5)}$$

In the above equations, $x=\mu^{1/3}=(2Q^6t/\tau_F)^{1/3}$ and $\Gamma(2/3)=1.254\,117\,94$.

APPENDIX C: SAMPLING FROM WEIGHTED DISTRIBUTIONS

During the MC procedures, it is sometimes necessary to map a randomly sampled uniform distribution into a randomly sampled weighted distribution specified by a particular function. Consider the sphere shown in Fig. 2(a). Using spherical polar coordinates, randomly sampled values of the polar angle, θ, must be weighted according to the normalized distribution,

$$P(\theta) = \tfrac{1}{2}\sin\theta. \quad \text{(C1)}$$

This is conceptually accomplished by equating the value of a uniformly sampled interval to the value of the incomplete integral of $P(\theta)$ determined by the upper limit, θ'

$$F=\frac{1}{2}\int_0^{\theta'} P(\theta)d\theta=\frac{1}{2}[1-\cos\theta']. \quad \text{(C2)}$$

In Eq. (C2), F is a uniform random variable sampled from the range, [0,1]. The choice of θ' is then determined by inverting Eq. (C2)

$$\theta'=\text{acos}[1-2\cdot F]. \quad \text{(C3)}$$

This mapping of the uniform distribution, F, into the weighted distribution, $\sin\theta$, is illustrated in Fig. 2(b).

The other type of mapping used in this work determines the number of chromophores on a given micelle (n) from the normalized Poisson distribution,

$$P(n)=\frac{e^{-\nu}\nu^n}{n!}. \quad \text{(C4)}$$

Because of the discretized nature of $P(n)$, an incomplete sum is used in place of the incomplete integral described by Eq. (C2)

$$F=\sum_{n=0}^{n'} P(n)=e^{-\nu}\sum_{n=0}^{n'}\frac{\nu^n}{n!}. \quad \text{(C5)}$$

A table of values in the interval [0,1] is constructed from Eq. (C5), each entry corresponding to subsequently increasing integral values of n'. The uniform random variable, F, is then looked up from this "list" of values to obtain the Poisson weighted value for n'.

APPENDIX D: PERIODIC BOUNDARY CONDITIONS, MINIMUM IMAGE CONVENTION, AND THE SPHERICAL CUTOFF

The combined use of periodic boundary conditions and the minimum image convention are employed extensively throughout the MC simulations. Although these techniques are thoroughly documented,[22] we wish to clarify the essential applications toward generating viable clustered chromophore configurations.

The coordinates of the hard sphere micelle centers are initially selected randomly in a box of side length L. (This is the central box shown in Fig. 3.) During the equilibration process, the spheres are sequentially allowed to take small steps, sometimes colliding with one another, sometimes moving outside the box boundary. After each equilibration step, the coordinates are transformed using the prescription,

$$\begin{aligned}&\text{if } r_{\alpha i}>L/2, \quad r_{\alpha i}\rightarrow r_{\alpha i}-L/2,\\ &\text{if } r_{\alpha i}<-L/2, \quad r_{\alpha i}\rightarrow r_{\alpha i}+L/2.\end{aligned} \quad \text{(D1)}$$

In Eq. (D1), α represents any of the three orthogonal Cartesian components of the micelle centers. This transformation has the effect of placing the image boxes shown in Fig. 3 about the original box (periodic boundary condition). If a micelle should wander outside one of the boundaries, another micelle will simultaneously move accross the opposite boundary from an image box. The distances between hard sphere centers are always measured using the minimum image convention. This constructs an image box of image spheres (dotted lines in Fig. 3) about the sphere in question.

$$\begin{aligned}&\text{if } r_{\alpha ij}>L/2, \quad r_{\alpha ij}\rightarrow r_{\alpha ij}-L/2,\\ &\text{if } r_{\alpha ij}<-L/2, \quad r_{\alpha ij}\rightarrow r_{\alpha ij}+L/2.\end{aligned} \quad \text{(D2)}$$

For any particular sphere i, the minimum image distance to any other sphere j is given by Eq. (D2).

Once the equilibration process is completed, chromophore coordinates are selected to lie randomly on the surfaces of the hard spheres. The number of chromophores on each sphere is chosen randomly from the Poisson distribution as described in Appendix C. The chromophore coordinates are transformed from spherical polar to absolute Cartesian coordinates with respect to the origin of the central box. The numbering of the chromophores is arbitrary and the one labeled 1 is designated the initial donor. A minimum image box of chromophores is then constructed using Eq. (D2), with chromophore 1 located at the origin. In Fig. 3, spheres that contain chromophores inside the minimum image are shaded in. The total number of chromophores considered in the EET calculation is then limited using the spherical cutoff. In Fig. 3, only the spheres labeled 1 through 4 have their centers inside the shell with radius R_{CO}. Consequently, only chromohores on these spheres are considered in the final EET calculation.

[1] A. V. Barzykin, Chem. Phys. **163**, 1 (1992).
[2] A. H. Marcus and M. D. Fayer, J. Chem. Phys. **94**, 5622 (1991).
[3] H. Bassler, *Hopping and Related Phenomenon* (World Scientific, Singapore, 1990), pp. 491.
[4] J. D. Byers, W. S. Parsons, R. A. Friesner, and S. E. Webber, Macromolecules **23**, 4835 (1990).
[5] K. P. Ghiggino, T. A. Smith, and G. J. Wilson, J. Mod. Opt. **37**, 1789 (1990).
[6] W. S. Struve, J. Opt. Soc. Am. B **7**, 1586 (1990).
[7] I. Yamazaki, N. Tamai, and T. Yamazaki, J. Phys. Chem. **94**, 516 (1990).
[8] T. P. Causgrove, Y. Shumei, and W. S. Struve, J. Phys. Chem. **93**, 6844 (1989).
[9] P. A. Afinrud, D. E. Hart, and W. S. Struve, J. Phys. Chem. **92**, 4067 (1988).
[10] M. K. Gibbons, D. E. Logan, and P. A. Madden, Phys. Rev. B **38**, 7292 (1988).
[11] J. Baumann and M. D. Fayer, J. Chem. Phys. **85**, 4087 (1986).
[12] G. H. Fredrickson, H. C. Andersen, and C. W. Frank, J. Poly. Sci. **23**, 591 (1985).
[13] J. Klafter and A. Blumen, J. Lumin. **34**, 77 (1985).
[14] K. A. Peterson, A. D. Stein, and M. D. Fayer, Macromolecules **23**, 111 (1990).
[15] M. D. Ediger, R. P. Domingue, and M. D. Fayer, J. Chem. Phys. **80**, 1246 (1984).
[16] A. H. Marcus, N. A. Diachun, and M. D. Fayer, J. Phys. Chem. **96**, 8930 (1992).
[17] A. H. Marcus, N. A. Diachun, and M. D. Fayer, Macromolecules **26**, 3041 (1993).
[18] D. L. Huber, Phys. Rev. B **20**, 2307 (1979).
[19] D. L. Huber, Phys. Rev. B **20**, 5333 (1979).
[20] A. Blumen, J. Chem. Phys. **72**, 2632 (1980).
[21] In Ref. 16, the micelles were incorrectly assumed to be randomly distributed in solution. This was a consequence of placing the micelle centers at the sites of a cubic lattice according to a binomial distribution. In order to avoid spatial overlaps, the lattice spacing was set equal to the micelle diameter. This is an acceptable approximation for low packing densities, but becomes increasingly inadequate for the higher densities under consideration (e.g., 5%–20%). For this reason, a con-

tinuum model is adopted in the present work to describe the relative spatial positions of the micelles.

[22] M. P. Allen and D. J. Tildesley, *Computer Simulation of Liquids* (Oxford University, Oxford, 1987).

[23] In general, the configuration is defined by the set $\mathbf{K}=\{\mathbf{r},\omega,\epsilon\}$, containing the probe coordinates, absolute orientations, and site energies. In a dynamic system, **K** may evolve in time. However, depending on the relative time scale of the energy transport observable in comparison to that of the evolution of **K**, suitable approximations may be applied to accurately model both ergotic and nonergotic systems. For nondispersive systems, such as those presented in this work, the EET is independent of site energy disorder and only a function of distance and orientation. The orientational dependence of the EET can be effectively accounted for by scaling the Förster transfer distance, R_0, by the factor, $\gamma^{1/2}$, which contains geometrical considerations.

[24] S. W. Haan and R. Zwanzig, J. Chem. Phys. **68**, 1879 (1978).

[25] E. L. Quitevis, A. H. Marcus, and M. D. Fayer, J. Phys. Chem. **97**, 5762 (1993).

[26] M. D. Fayer (to be published).

[27] M. D. Ediger and M. D. Fayer, J. Chem. Phys. **78**, 2518 (1983).

[28] G. A. Baker, Jr. and P. Groves-Morris, *Encyclopedia of Mathematics and its Applications* (Addison-Wesley, Reading, 1981), Vol. 13.

[29] W. R. Smith and D. Henderson, Mol. Phys. **19**, 411 (1970).

[30] L. Verlet and J. Weiss, Phys. Rev. A **5**, 939 (1972).

[31] R. F. V. Anderson, *Introduction to Linear Algebra* (Holt, Rinehart, and Winston of Canada, New York, 1986).

[32] W. H. Press, B. P. Flannery, S. A. Teukolsky, and W. T. Vetterling, *Numerical Recipes in C: The Art of Scientific Computing* (Cambridge University, Cambridge, 1988).

[33] M. Tachiya, *Kinetics of Nonhomogeneous Processes*, edited by G. R. Freeman (Wiley, New York, 1987), pp. 575.

[34] G. Marsaglia and A. Zaman, J. Appl. Prob. **1**, 1 (1991).

[35] F. James, Comp. Phys. Comm. **60**, 329 (1990).

[36] K. A. Peterson and M. D. Fayer, J. Chem. Phys. **85**, 4702 (1986).

[37] P. Ekwall, L. Mandell, and K. Fontell, *Molecular Crystals and Liquid Crystals* (Gordon and Breach Science, Printed in Great Britain, 1969), Vol. 8; pp. 157.

[38] A. H. Marcus and M. D. Fayer (to be published).